

2 mit

NASA TECHNICAL MEMORANDUM

NASA TM X- 64786

(NASA-TM-X-64786) THE DEVELOPMENT OF A
TWO-COMPONENT FORCE DYNAMOMETER AND TOOL
CONTROL SYSTEM FOR DYNAMIC MACHINE TOOL
RESEARCH (NASA) 47 p HC \$4.50 CSCL 14B

N73-33371

Unclass

G3/14 19861

THE DEVELOPMENT OF A TWO-COMPONENT FORCE
DYNAMOMETER AND TOOL CONTROL SYSTEM
FOR DYNAMIC MACHINE TOOL RESEARCH


By Ian Alexander Sutherland
Process Engineering Laboratory

May 23, 1973



NASA

*George C. Marshall Space Flight Center
Marshall Space Flight Center, Alabama*

1. REPORT NO. NASA TM X-64786	2. GOVERNMENT ACCESSION NO.	3. RECIPIENT'S CATALOG NO.	
4. TITLE AND SUBTITLE The Development of a Two-Component Force Dynamometer and Tool Control System for Dynamic Machine Tool Research		5. REPORT DATE May 23, 1973	
		6. PERFORMING ORGANIZATION CODE	
7. AUTHOR(S) Ian Alexander Sutherland*		8. PERFORMING ORGANIZATION REPORT #	
9. PERFORMING ORGANIZATION NAME AND ADDRESS George C. Marshall Space Flight Center Marshall Space Flight Center, Alabama 35812		10. WORK UNIT NO.	
		11. CONTRACT OR GRANT NO.	
12. SPONSORING AGENCY NAME AND ADDRESS National Aeronautics and Space Administration Washington, D. C. 20546		13. TYPE OF REPORT & PERIOD COVERED Technical Memorandum	
		14. SPONSORING AGENCY CODE	
15. SUPPLEMENTARY NOTES Prepared by Process Engineering Laboratory, Science and Engineering *Dr. I. A. Sutherland received his Ph. D. from the University of Bristol, England, in the field of metal cutting. This work was authored while he held an NRC Resident Research Associateship at Marshall Space Flight Center.			
16. ABSTRACT The increasing demands for higher production rates necessitate a deeper knowledge of the metal cutting process under dynamic machining conditions. This work describes the successful development of a tooling system that makes a controlled sinusoidal oscillation, simulating a dynamic chip removal condition, and measures the machining forces in two mutually perpendicular directions without any cross sensitivity.			
17. KEY WORDS		18. DISTRIBUTION STATEMENT Unclassified-Unlimited  DR. M. P. L. SIEBEL Director, Process Engineering Laboratory	
19. SECURITY CLASSIF. (of this report) Unclassified	20. SECURITY CLASSIF. (of this page) Unclassified	21. NO. OF PAGES 47	22. PRICE NTIS

ACKNOWLEDGMENT

This report resulted from work accomplished while the author held a National Research Council Resident Research Associateship. The author would like to thank the Associateship directors, Drs. Thomas H. Curry and Roland W. Kinney, and the coordinator for the Associateship Program at Marshall, Dr. George C. Bucher, for their encouragement and support.

The author wishes to express his thanks to the many people in the host laboratory, Process Engineering, who have offered continued support and faultless assistance; in particular Mr. Wilhelm Angele for his counsel in scientific matters.

The author is indebted to Dr. Mathias P. L. Siebel, who, in his capacity as scientific advisor, has been a source of endless inspiration and, as laboratory director, has provided every facility for this work to be carried out.

TABLE OF CONTENTS

	Page
INTRODUCTION.	1
DESCRIPTION	1
Force Dynamometer	1
Foreward	1
Objective	2
Theory	2
Requirements	4
Design	5
Detailed Design	8
Electrical Design	9
Calibration	10
Tool Control System	13
Objective	13
Tool Vibration	14
Design of Flexible Tooling	14
Theory	17
Open Loop Tests	20
Closed Loop Tests	21
CONCLUSIONS.	22
APPENDIX A.	29
APPENDIX B.	32
REFERENCES	36

LIST OF ILLUSTRATIONS

Figure	Title	Page
1.	Schematic representation of a dynamometer and its support. . . .	3
2.	Schematic of two-component force dynamometer	5
3.	"I" section strut showing design notation and position of strain gauges	6
4.	Typical bridge circuitry adding gauges in thrust direction	7
5.	Static calibration in cutting direction	11
6.	Static calibration in thrust direction	12
7.	Schematic of basic tool control system.	15
8.	Schematic of force dynamometer housing, giving analytical notation	16
9.	Schematic arrangement of the vibrator and flexible tooling	18
10.	System response with displacement feedback only	23
11.	System response with velocity feedback only	24
12.	System response with displacement and velocity feedback	25
13.	System response with displacement and velocity feedback — after modification.	26
14.	Closed loop response — comparing measured results with predicted	27
15.	View of force dynamometer and flexible tooling showing completed assembly	28
A-1.	Notch geometry	30
B-1.	Flexible hinge geometry and notation	32
B-2.	Notation of vibrating system.	34

LIST OF TABLES

Table	Title	Page
1.	Frequency Range for Which the Open Loop Response Exceeds the Given Values of v_o/v	21

DEFINITION OF SYMBOLS

Equations are presented in numerical order in the text and the symbols used are listed below with their notation.

Subscripted symbols not shown below will obey the general subscript notation.

<u>Symbol</u>	<u>Definition</u>
A	Ratio of feedback to error signal amplitude (open loop)
a	$\sqrt{R_n t_m}$
a _c	Moment arm of cutting force (P_c) about strut C
a _t	Moment arm of thrust force (P_t) about struts A and B
b	Width
c	Damping constant
D	Deflection
d	Thickness of hinge strut
d _n	Deflection of notch
d _s	Deflection of strut
E	Modulus of elasticity
F	Force
f	Damping coefficient, also frequency
G	Amplifier gain
h	Distance between struts C and D
I _h	Second moment of area of hinge

DEFINITION OF SYMBOLS (Continued)

<u>Symbol</u>	<u>Definition</u>
k	Stiffness
L	Combined notch and strut length of dynamometer housing
L_1	Length of strut
L_2	Length of notch
L_b	Length between bolt holes on flange
L_f	Length between flanges ("I" section struts)
M	Ratio of feedback to control amplitude (closed loop), also bending moment
M^*	Equivalent mass
P	Force
p	Moment arm from "O" to vibrator axis (hinge)
"Q"	Vibration term describing amount of damping in system
q	Moment arm from "O" to tool axis (hinge)
R	Dummy resistance
R_n	Radius of curvature of housing notch
r	Ratio of toolholder to housing mass (m_1/m_2)
s	Frequency operator
T	Vibrator transfer coefficient
T_f	Flange thickness ("I" section strut)
T_h	Torque on hinge

DEFINITION OF SYMBOLS (Continued)

<u>Symbol</u>	<u>Definition</u>
T_s	Strut thickness (force dynamometer housing)
$T(s)$	Transfer function
t	Strut thickness at displacement (y) also time
t_1	Thickness of "I" section strut
t_2	Thickness of "I" section notch
t_m	Minimum thickness of housing notch
v	Error signal
v_i	Control signal
v_o	Feedback signal
v'	Error signal after amplification (G)
X	Displacement amplitude
x	Displacement vector
y	Displacement scalar
α	Ratio of strut length to notch radius of curvature
ϵ	Strain
Θ	Hinge angular rotation
λ	Phase between feedback and control signal (closed loop)
ϕ	Phase between feedback and input signal (open loop)
σ	Strain over gauge length
ω	Angular frequency
l	Length of hinge strut

DEFINITION OF SYMBOLS (Concluded)

<u>Symbol</u>	<u>Definition</u>
<u>General Subscripts</u>	
A	Gauge A
B	Gauge B
b	Bending
C	Gauge C
c	In the cutting direction
cp	Compressive
D	Gauge D
d	Dynamometer
f	Flange
h	Hinge
i	Inertia
m	Measured
mi	Measured including inertia
T	Temperature
t	In the thrust direction
tr	Torsional
v	Vibrator
1	Of the dynamometer mounting structure
2	Of the dynamometer measuring element

THE DEVELOPMENT OF A TWO-COMPONENT FORCE DYNAMOMETER AND TOOL CONTROL SYSTEM FOR DYNAMIC MACHINE TOOL RESEARCH

INTRODUCTION

The need for research into machining processes is widely recognized. Production rates are often limited by self-excited vibration, commonly known as chatter, which results from the dynamic interaction between the metal cutting process and the machine tool structure. Vibration causes increased tool wear; dimensional inaccuracies; a poor surface finish, and can be extremely noisy.

The increasing demand for higher production rates necessitates a deeper knowledge of the cutting forces under dynamic machining conditions so that the parameters affecting machine tool instability, or chatter, can be established.

The objective of the work described in this report was to design and develop a tooling system that would both measure the machining forces in the cutting and thrust directions and oscillate in a controlled manner to simulate a dynamic chip removal process.

DESCRIPTION

Force Dynamometer

Foreword. Care has to be taken when designing a dynamic force dynamometer to maintain the proportionality between the strain in the measuring element and the applied force. Kegg [1] has shown in general terms how the natural frequencies of the dynamometer mounting system and the machine tool structure may affect the output signal. Komanduri, et al, [2] substantiated Kegg's findings and recommended dynamic calibration with the dynamometer mounted on the machine tool structure. They further explained that if the

measuring element mass was kept small in comparison to the mounting structure mass then proportionality between strain and applied force would be assured. Examining the theory will show why.

Objective. A force dynamometer which has to measure machining forces needs to be part of the tooling or workpiece system. For convenience, the stationary component is used as the dynamometer so that for multiedged machining operations such as milling, the dynamometer is used as the workpiece holder [3], whereas most single-point operations, such as turning, require using the dynamometer mass as the toolholder. This section of the report will concentrate on the design of a force dynamometer for a turning situation, where only orthogonal cutting will be considered. The dynamometer therefore need only measure forces in two mutually perpendicular directions in the plane of rotation, i. e., for convenience, one in the cutting direction — tangential to the workpiece at the tool, and the other in the thrust direction — radial to the workpiece at the tool. The design should try to minimize cross sensitivity, whereby a force in the cutting direction results in a reading, and hence an apparent force, in the thrust direction. In this way, direct force readings can be achieved without having to make corrections or solve simultaneous equations.

The high forces and tool tip temperatures that are characteristic of a machining operation require a design that is stiff and has temperature compensation. However, the design also needs to detect the lower magnitude oscillatory forces and so has to have a high sensitivity.

The final design will be incorporated in the tool control system that will be described beginning on page 13.

Theory. The dynamometer measuring and support system can be represented for analytical purposes as shown in Figure 1.

When subjected to an oscillatory applied force F_2 the equations of motion become:

$$m_2 \ddot{x}_2 + k_2 (x_2 - x_1) + f_2 (\dot{x}_2 - \dot{x}_1) = F_2 \quad (1)$$

$$m_1 \ddot{x}_1 + k_1 x_1 + f_1 \dot{x}_1 - k_2 (x_2 - x_1) - f_2 (\dot{x}_2 - \dot{x}_1) = 0 \quad (2)$$

$$\text{Let } x = X e^{ist} \text{ and } F = F e^{ist} \quad (3)$$

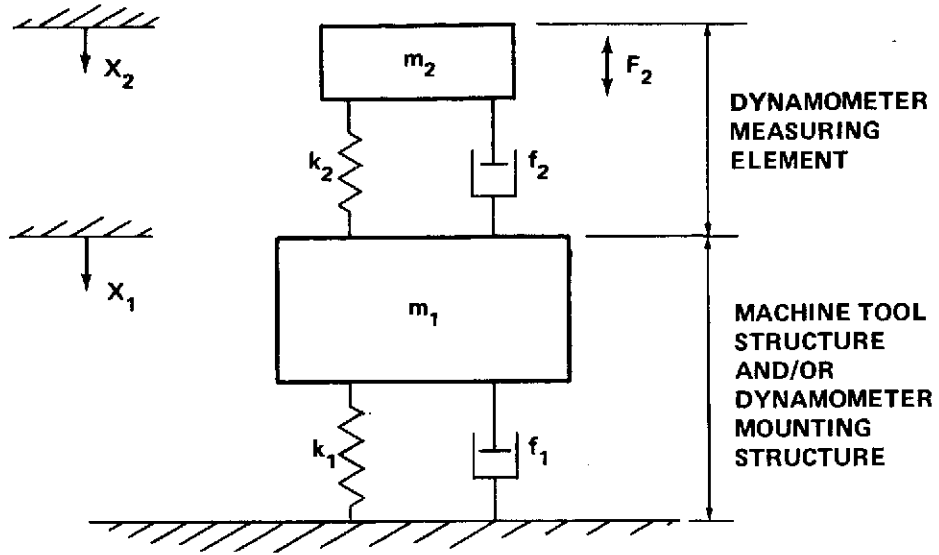


Figure 1. Schematic representation of a dynamometer and its support.

where $i = \sqrt{-1}$ and s is a frequency operator and t is time. Then, after algebra, the dynamometer output to force input can be expressed as

$$\frac{x_2 - x_1}{F_2} = \frac{1}{m} \left[\frac{\omega_1^2 + 2c_1\omega_1 is - s^2}{\omega_1^2\omega_2^2 + (2c_1\omega_1\omega_2^2 + 2c_2\omega_2\omega_1^2) is - [\omega_1^2 + \omega_2^2(1+r) + 4\omega_1\omega_2 c_1 c_2] s^2 - [\omega_1 + \omega_2(1+r)] is^3 + s^4} \right] \quad (4)$$

where:

$$\begin{aligned} \omega_1 &= \sqrt{k_1/m_1} & c_1 &= f_1/2\sqrt{m_1 k_1} & r &= m_2/m_1 \\ \omega_2 &= \sqrt{k_2/m_2} & c_2 &= f_2/2\sqrt{m_2 k_2} \end{aligned}$$

ω_1 and ω_2 are the undamped natural frequencies of each of the spring, mass systems. Resonances and antiresonances will occur when the respective denominator and numerator is zero. It can be seen that an antiresonance occurs when $s = \omega\sqrt{1-c_1^2}$ and a resonance will occur at a frequency slightly below this [1].

If the ratio r of the measuring element mass to the mounting system mass is negligible in comparison with unity then the denominator in equation (4) can be factored and becomes:

$$\frac{X_2 - X_1}{F_2} = \frac{1}{m_2} \left[\frac{1}{\omega_2^2 + 2c_2 \omega_2 is - s^2} \right] , \quad (5)$$

Therefore, if the mass of the dynamometer element is small compared with the mass of the mounting structure, then the dynamometer will be independent of the characteristics of the mounting structure.

Another aspect to be considered is the forcing of the structure directly through the workpiece. This would be equivalent to letting the oscillatory force F_2 act on the mounting system mass (m_1) in Figure 1, in which case the equations of motion reduce to:

$$\frac{X_1}{X_2} = \frac{\omega_2^2 + 2c_2 \omega_2 is - s^2}{\omega_2^2 + 2c_2 \omega_2 is} \quad (6)$$

If $\omega_2 \gg s$, then X_1 and X_2 would be equal in magnitude and the dynamometer would be isolated from disturbances to its mounting system. The natural frequency of the dynamometer, therefore, should be well above the operating frequency range.

Requirements.

1. Low dynamometer mass — to minimize the effect of the mounting structure and reduce inertia corrections,
2. High element stiffness — to withstand high machining forces and to combine with 1. above to create a natural frequency high enough to ensure vibration isolation from the mounting structure,
3. High sensitivity — to detect lower magnitude oscillatory forces,
4. Minimal cross sensitivity — to ensure ease of operation and data analysis, avoiding the solution of two simultaneous equations before obtaining the machining forces, and
5. Temperature compensation — so that the high temperatures generated by the machining process and the consequential heat flow through the strain-gauged elements do not affect the dynamometer sensitivity.

Design. Apart from the listed design requirements there are a number of mechanical considerations. The dynamometer mass will be utilized as a tool-holder for cutting tests machining a square-threaded helical workpiece. Only orthogonal cutting will be considered so that the toolholder assembly should be mounted perpendicularly to the turning axis of the machine tool.

The force dynamometer is shown schematically in Figure 2. The toolholder is kinetically constrained with strain gauges A and B adding to give the thrust force and gauges C and D adding to give the cutting force. Temperature compensation can be achieved by mounting passive gauges perpendicularly to the active ones (Fig. 3) and wiring them in opposite arms of the bridge (Fig. 4).

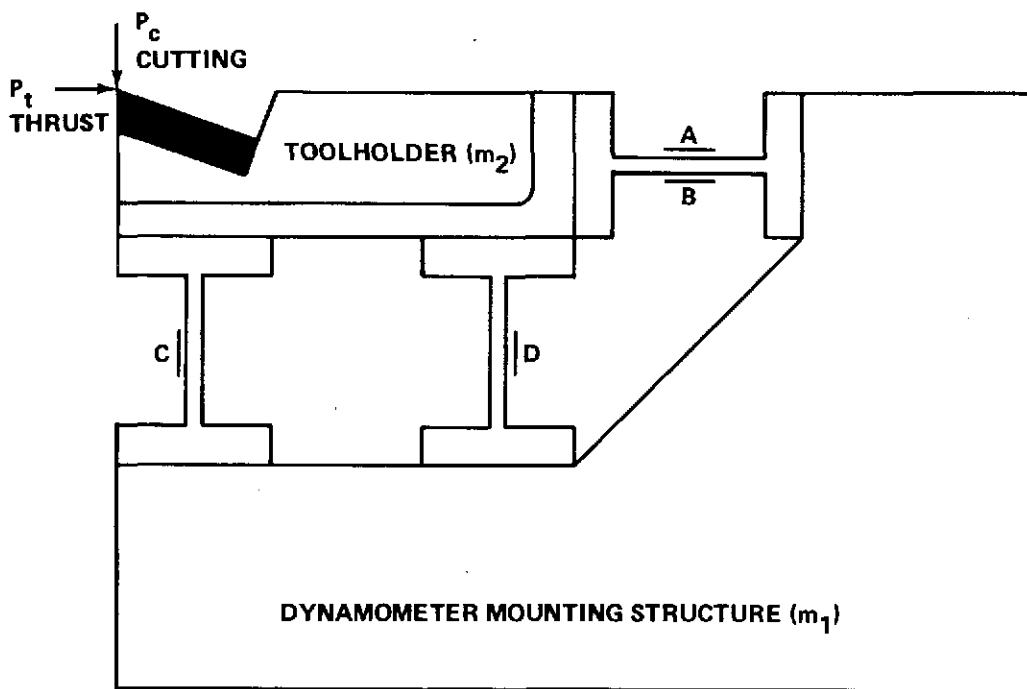


Figure 2. Schematic of two-component force dynamometer.

The toolholder mass is minimized by using a light but stiff material such as Beryllium.

The conflicting requirements of stiffness and sensitivity necessitate using semiconductor strain gauges and high gain amplification.

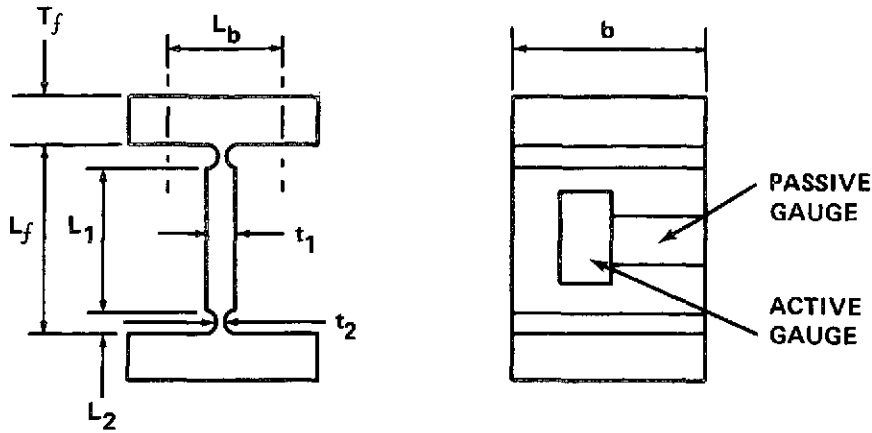


Figure 3. 'I' section strut showing design notation and position of strain gauges.

Cross sensitivity generally arises due to compressive forces in gauges C and D, for example, resulting in bending forces in gauges A and B. The notches in the 'I' section struts shown in Figure 3 allow bending at the notch rather than over the gauge length with no significant effect on the compressive stiffness of the strut.

Further cross coupling can arise from the relative placing of the struts with respect to the applied force. If we assume that A, B, C and D are the gauge outputs for respective strut forces F_A , F_B , F_C , F_D , then for a cutting force (P_c) in Figure 2:

$$\text{Resolving:} \quad F_C + F_D = P_c ; F_A + F_B = 0 \quad (7)$$

$$\text{Moments about the intersect of struts A and D:} \quad F_C = P_c \frac{(h + a_c)}{h} ; F_D = \frac{-P_c a_c}{h} \quad (8)$$

where h is the distance between struts C and D; a_t is the moment arm of the thrust force (P_t) above the strut AB and a_c is the moment arm of the cutting for (P_c) outside the strut C.

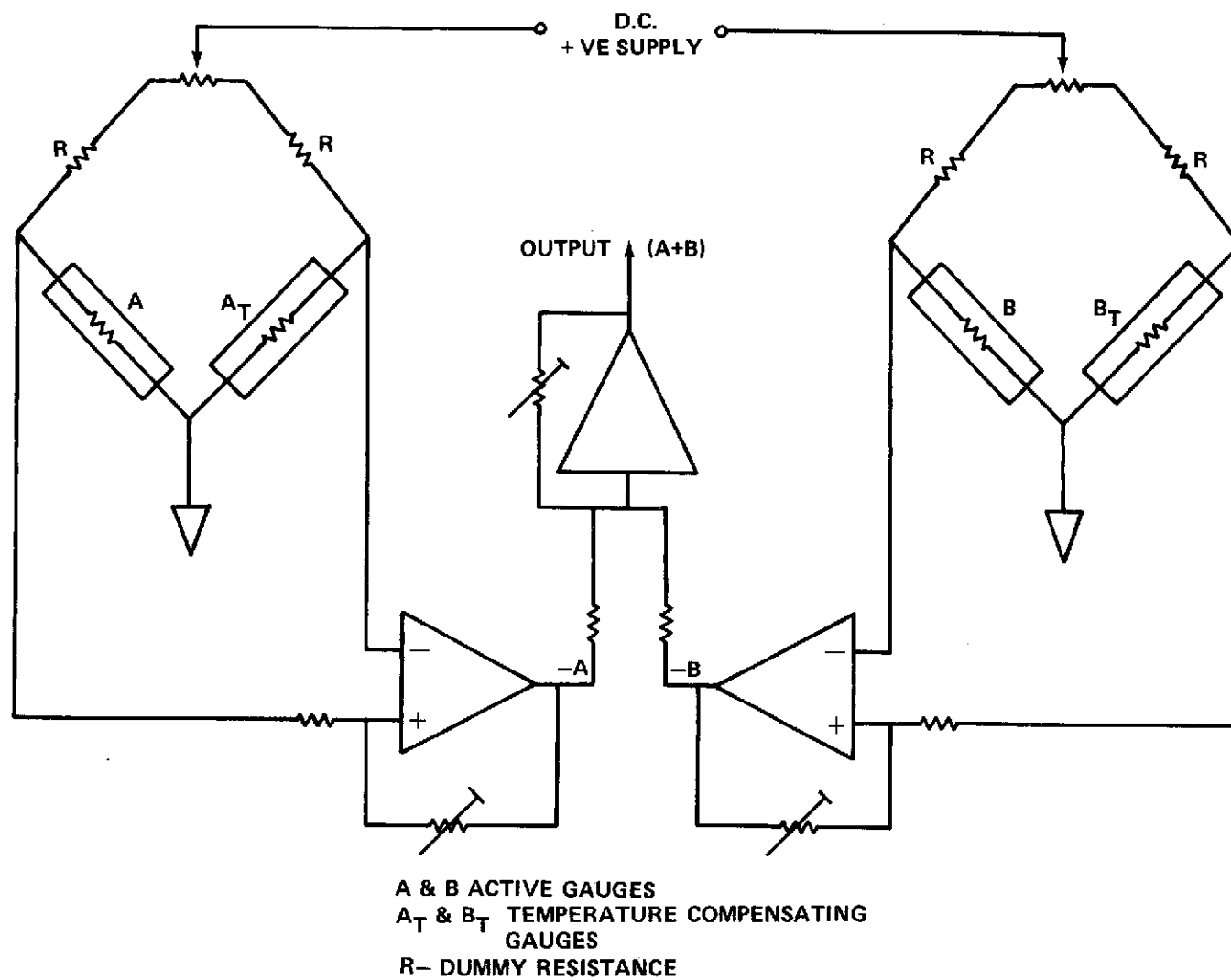


Figure 4. Typical bridge circuitry adding gauges in thrust direction.

For a thrust force (P_t) in Figure 2 then:

$$\text{Resolving:} \quad F_A + F_B = P_t ; F_C + F_D = 0 \quad (9)$$

Moments about the intersect
of struts A and D:

$$F_C = -\frac{P_t a_t}{h} ; F_D = +\frac{P_t a_t}{h} \quad (10)$$

It can be seen from the above equations that geometrical cross coupling only arises from a thrust force (P_t) and will be negligible if the moment arm (a_t) is zero; i.e., if the tool tip is in line with the strut AB. If this is not possible then provided the gauge factors of C and D are identical and the gauges are wired to add, then the cross coupling forces ($P_t \cdot a_t / h$) in equation (10), that are opposite in polarity, will be electrically eliminated.

For minimal cross coupling, therefore, it is essential that the gauge outputs A, B, C and D be identical for a given strut force. The strut thickness (t_1) must be the same for all struts, and gauges should be in matched sets. Possible electrical compensation will be discussed under electrical design.

Detailed Design. The following quantities were calculated using the nomenclature of Figure 3:

$$\text{Compressive stiffness } (k_{cp}) = \frac{Eb}{2L_2/t_2 + L_1/t_1} \quad (11)$$

$$\text{Bending stiffness } (k_b) = \frac{Eb}{(L_1/t_1)^3 - (L_1/t_2)^3 + (L_f/t_2)^3} \quad (12)$$

assuming the strut flanges are encastré and displaced in opposite directions.

$$\text{Strain over gauge length } (\sigma) = \frac{1}{bt_1 E} \quad (13)$$

$$\text{Flange stiffness } (k_f) = \frac{16EbT_f^3}{L_b^3} \quad (14)$$

$$\text{Natural frequency } (\omega_2) = \frac{1}{2\pi} \sqrt{\frac{k_{cp}}{m_2}} \quad (15)$$

The following dimensions were used:

$$\begin{array}{ll}
 L_f = 0.025 \text{ m} & b = 0.025 \text{ m} \\
 L_1 = 0.023 \text{ m} & t_1 = 0.003 \text{ m} \\
 L_2 = 0.001 \text{ m} & t_2 = 0.0005 \text{ m} \\
 L_b = 0.006 \text{ m} & T_f = 0.006 \text{ m} \\
 m_2 = 0.250 \text{ kgms} & E = 2 \times 10^{11} \text{ N/m}^2 \text{ (Young's} \\
 & \text{Modulus)}
 \end{array}$$

The design data therefore becomes:

$$\begin{array}{ll}
 \text{Compressive stiffness} & = 4.28 \times 10^8 \text{ N/m} \\
 \text{Bending stiffness} & = 1.84 \times 10^5 \text{ N/m} \\
 \text{Ratio of compressive to bending stiffness} & = 2320 \\
 \text{Strain over gauge length} & = 0.03 \mu\text{strain/N} \\
 \text{Flange stiffness} & = 8.0 \times 10^{10} \text{ N/m} \\
 \text{Ratio of flange to compressive stiffness} & = 120 \\
 \text{Natural frequency (thrust)} & = 6.6 \text{ kc/s} \\
 \text{Natural frequency (cutting)} & = 9.3 \text{ kc/s}
 \end{array}$$

Electrical Design. Typical bridge circuitry for monitoring the forces in the thrust direction is shown in Figure 4.

There is a bridge for each active/passive gauge pair so that the respective outputs of A, B, C and D gauges can be monitored. In this way a check can be made on the contribution of each gauge during calibration. The dummy resistors (R) are chosen in matched pairs and should have resistive values near those of the strain gauges. The bridges also have a balancing facility. The bridge outputs are fed into operational amplifiers that have a fine-gain adjustment to compensate for any mismatch in the gauge sensitivities. The outputs are then added using another operational amplifier that has a gain adjustment for the overall cutting or thrust force sensitivity. The bridge outputs are then fed to the appropriate monitoring equipment.

In the present study, forces were recorded on an Ampex loop tape recorder and played back through a Honeywell Visicorder, an oscilloscope and an ac/dc rms-millivoltmeter.

Strain gauge specifications were as follows:

B. L. H. semiconductor strain gauges

Type:	SPB3-12-12
Gauge factor:	108 ± 2 percent
Gauge resistance (unbacked):	139 ± 1 percent at 25°C
Gauge length:	3.5 mms

Calibration. Calibration involves both static and dynamic forcing of the dynamometer. Static calibration checks on the linearity, sensitivity and cross sensitivity of the dynamometer while dynamic calibration determines whether the static calibration results can be used over the operating frequency range; i.e., that the operating range is away from the influences of any resonance or antiresonance associated with either the system or the mounting structure.

Static calibration curves for forces in the cutting direction are given in Figure 5 and show that the dynamometer is linear and that there is no cross coupling from the cutting to the thrust direction. It can be seen that gauge D is in tension, as predicted by equation (8).

Static calibration curves for forces in the thrust direction are given in Figure 6. They again demonstrate linearity and show that cross coupling from the thrust to the cutting direction, predicted in equation (10), is eliminated by the summing procedure.

These static tests demonstrate that the cross sensitivity is less than 1 percent in either direction and can be neglected.

Dynamic excitation of the system showed that over the operating range of 0-400 Hz there was no resonance or antiresonance due to the mounting system and that the resonant frequency of the dynamometer was only slightly less than anticipated. The high "Q" associated with this resonance indicated that (f_2) in equation (1) could be neglected so that only the inertia forces of the toolholder need be considered. If F_i represents the inertia force and F_m the force measured by the dynamometer; i.e., a force proportional to strain (ϵ), which is a function ($x_2 - x_1$) in equation (1), then equation (1) becomes:

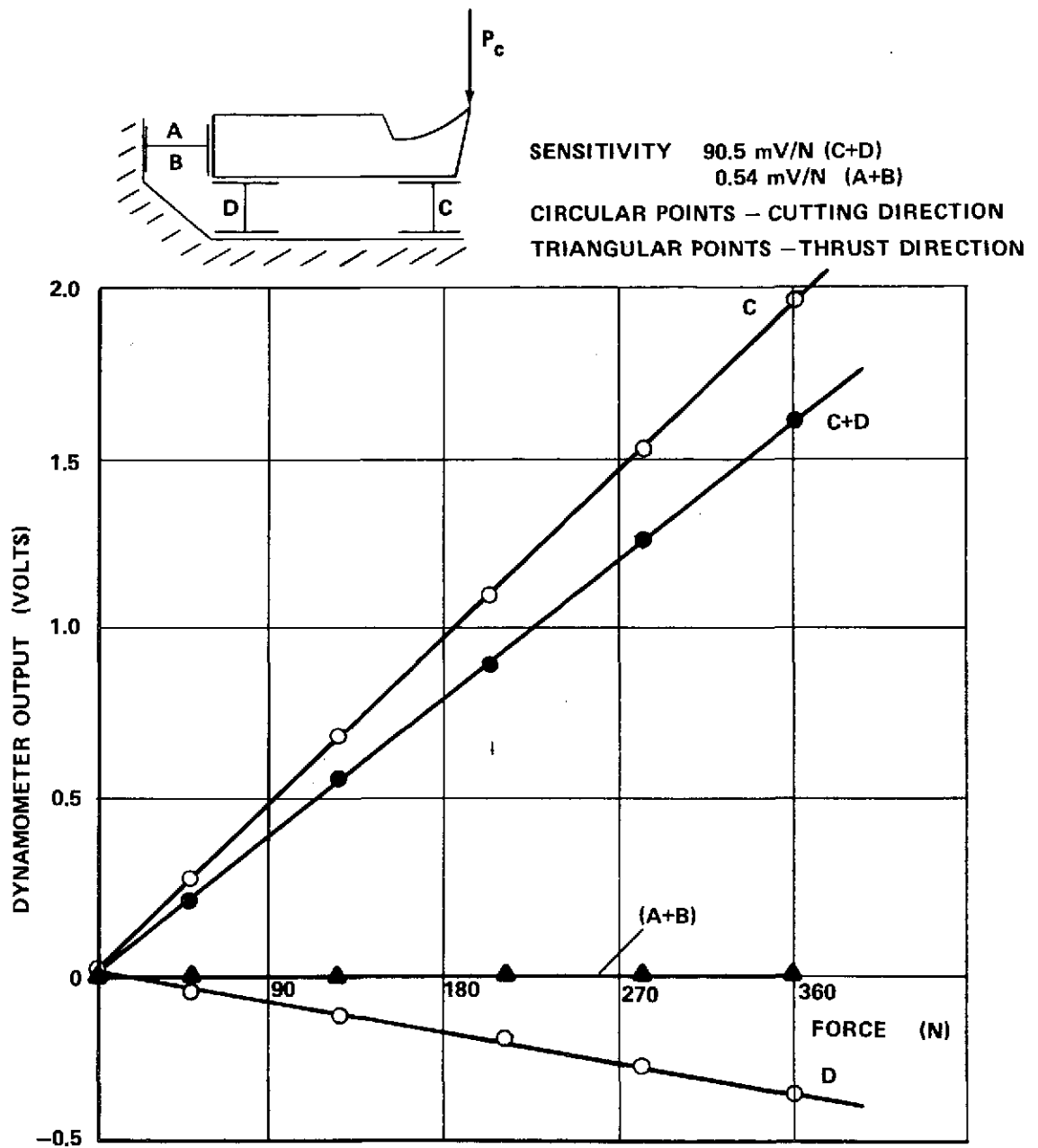


Figure 5. Static calibration in cutting direction.

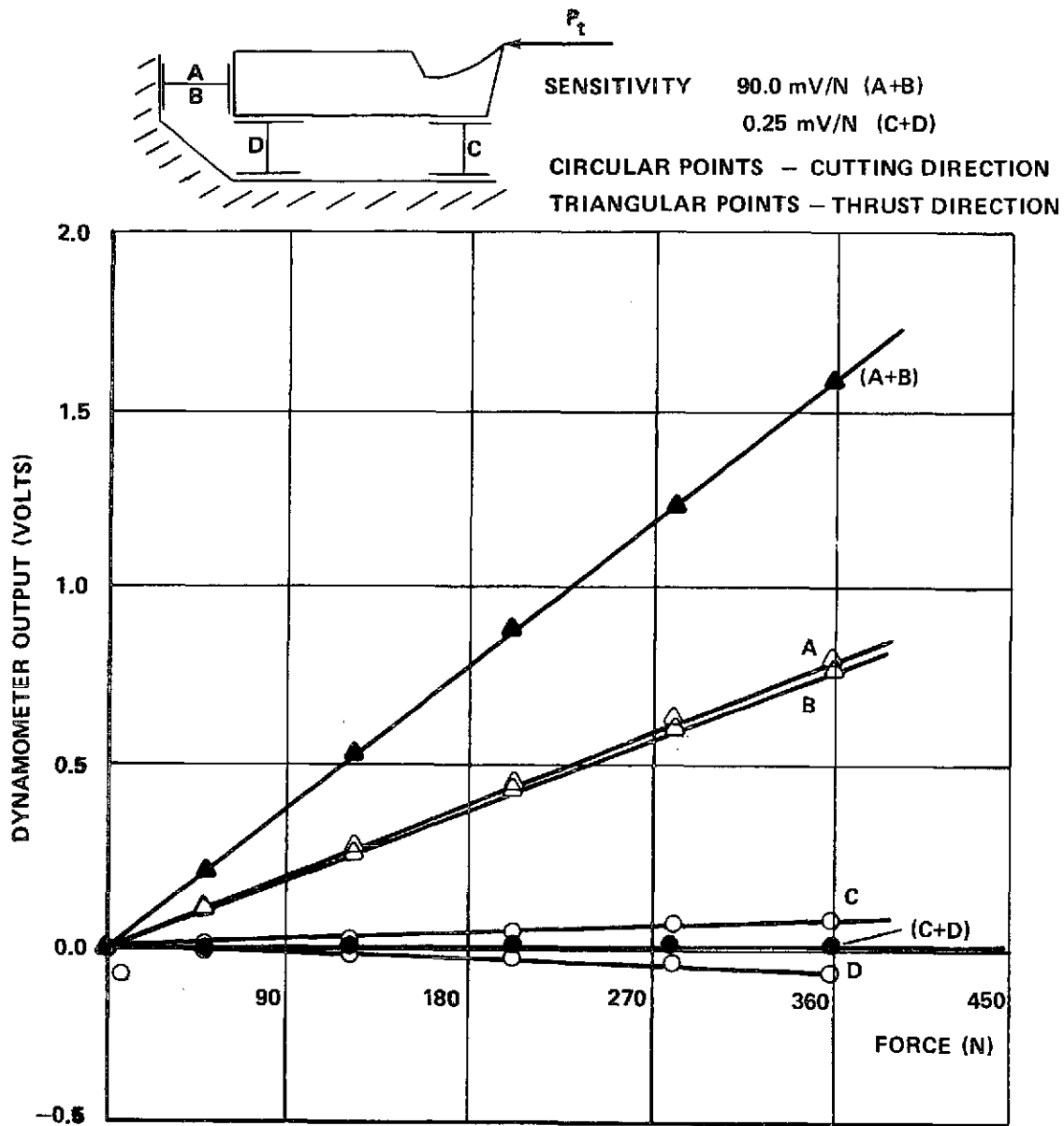


Figure 6. Static calibration in thrust direction.

$$\underline{F}_i + \underline{F}_m = \underline{F}_2 \quad (16)$$

where \underline{F}_i , \underline{F}_m and \underline{F}_2 are force vectors. Calibration assures that $\underline{F}_m = \underline{F}_2$ when $\underline{F}_i = 0$ and frequency $f = 0$.

Inertia forces can be measured when $\underline{F}_2 = 0$; i.e., when not cutting, in which case $\underline{F}_{mi} = -\underline{F}_i$. Substituting back in equation (16) gives:

$$\underline{F}_m - \underline{F}_{mi} = \underline{F}_2 \quad (17)$$

where \underline{F}_{mi} is the measured inertia force. The real dynamic force therefore is given when the measured inertia force is vectorially subtracted from the measured cutting force. In the present application, (m_2) in equation (1) was chosen to be small enough to neglect this correction below 150 Hz.

Tool Control System

Objective. Forces during machining, because of the elastic nature of a machine tool structure, cause a relative displacement between the tool and workpiece. This has the effect of changing the chip geometry and altering these cutting forces, which is why the cutting process and machine tool structure are so often described as dynamically interacting. This procedure can lead to instability of the machining process and severe uncontrolled vibration.

In order to evaluate how the machining forces arise and how they behave during this dynamic situation it is necessary to measure the machining forces while the tool vibrates in a controlled sinusoidal manner.

"Vibration" in the text of this report will imply a controlled sinusoidal oscillation rather than a random noise that is sometimes implied by other writers.

This simulation of a dynamic chip removal process requires a frequency range of 5 to 400 Hz and an amplitude range of 0 to 0.125 mm (5×10^{-3} in.).

The tooling system would need to be flexible to vibrate and yet stiff enough to remain isolated from the influence of the cutting forces and the possibility of self-excited vibration or chatter. These conflicting requirements necessitate developing a tool control system.

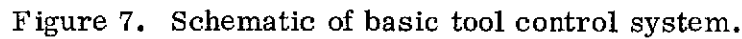
Tool Vibration. A tool can be vibrated in a number of ways, many of which are severely limited by frequency. Wallace and Andrew [4] used a gear driven eccentric cam to oscillate the cross slide of a lathe, but were restricted to frequencies below 15 Hz by the inertia of the system. Hydraulic vibrators are desirable because of their size and ease of mounting, but compressibility of the fluid and flexibilities of the fluid supply lines can cause resonances at the upper end of the required frequency range. Smith and Tobias [5], however, used an electromagnetic vibrator with a velocity feedback control system quite successfully, but neglected to mention any static deflection problems.

It was decided therefore to develop a system similar to Smith's with the addition of a displacement feedback for a high tool static stiffness (Fig. 7). After considering frequency, amplitude and inertia requirements, it was decided that a 675 N (150 lbf) electromagnetic vibrator was adequate for the cutting force levels anticipated.

The suspension of the tool dynamometer and its mounting, however, presents a problem because it has to be stiff in the cutting direction to withstand the high machining forces but flexible in the thrust direction so that the tool can vibrate. The design of the force dynamometer housing will be discussed next.

Design of Flexible Tooling. The design of the force dynamometer housing can be worked backwards from the required resonant frequency of the system. In order to offer the vibrator a balanced mechanical impedance the housing resonant frequency should fall midway between the operating frequency extremes of 5 to 400 Hz. If this resonance is chosen to be about 100 Hz, then the ratio of housing mass to bending stiffness is fixed.

The housing mass should be large in comparison with the dynamometer mass; i.e., $r = m_2/m_1 < 0.1$, — [see equations (4) and (5)] but the overall mass should be minimized to reduce inertia forces. The dynamometer mass is made as small as possible by using beryllium and the housing mass is reduced by machining away redundant material until its mass is about ten times that of the dynamometer. Once the combined mass is known the required bending stiffness of the housing is able to be calculated.



Once the required values of stiffness are known, design parameters can be optimized using the equations given in Appendix A. In the present application the ratio of compressive/bending stiffness is sufficiently high to merit adding notches to the housing leaf spring struts, as shown in Figure 8. The strut dimensions, therefore, are entirely governed by the compressive/bending stiffness requirement. The housing surrounding the dynamometer struts (Figs. 2 and 8) should be at least 100 times stiffer than the strut compressive stiffness of 4×10^8 N/m, in order to minimize cross sensitivity in the dynamometer.

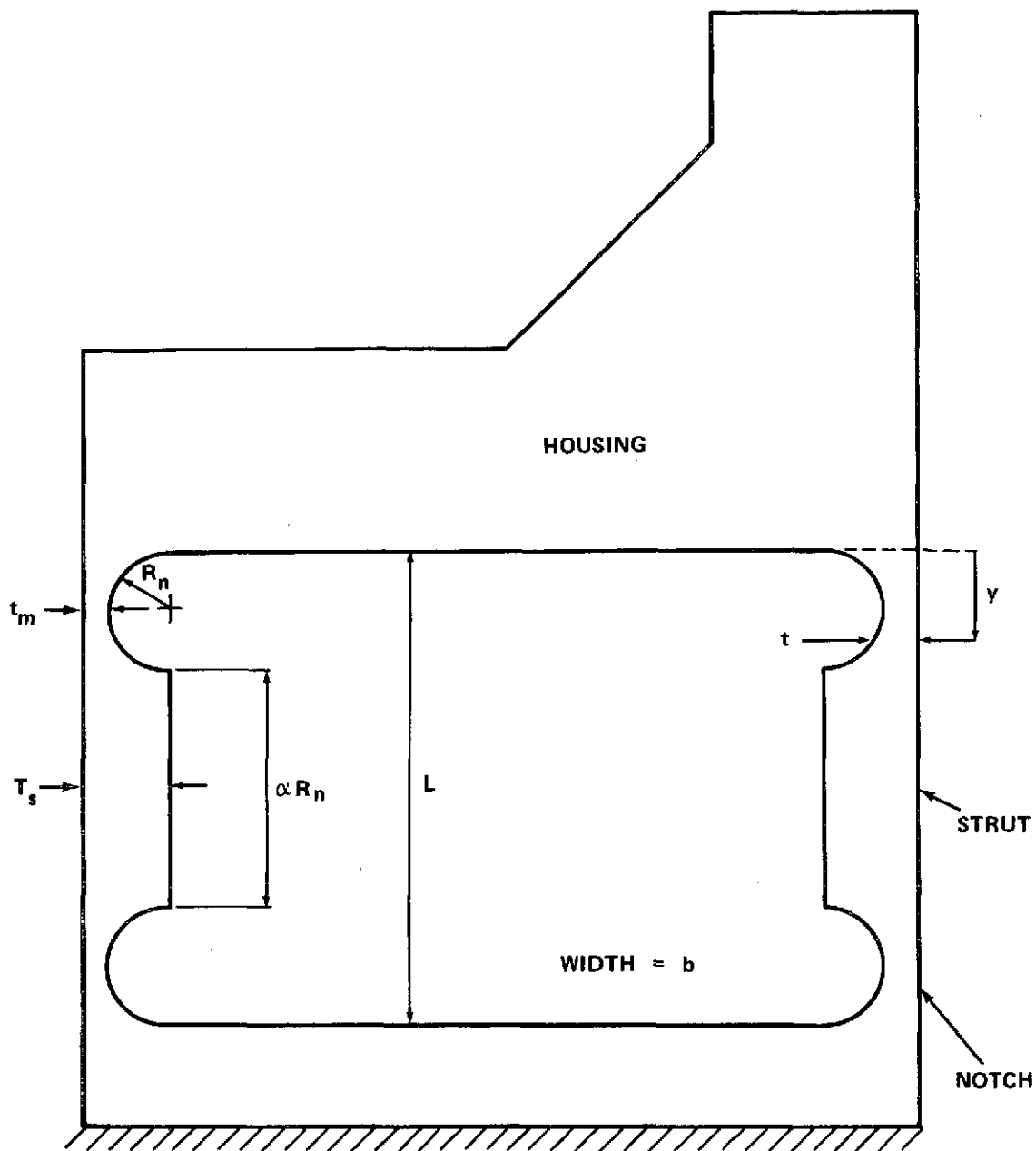


Figure 8. Schematic of force dynamometer housing, giving analytical notation.

The final design requirement is to mount the vibrator behind the dynamometer and form a solid linkage with the vibrator table. With the vibrator used in this present application weighing 1575 N (350 lbf) and measuring 0.6 m by 0.38 m dia. (24 in. by 15 in. dia.), in-line mounting tended to bend the cross slide due to the center of gravity being outside the bed rails, and so

it was decided to mount the vibrator vertically as shown in Figure 9 and excite the dynamometer by transferring the motion through 90 deg using a mechanical hinge. As the design of this hinge is not entirely relevant to this report it is given in Appendix B.

It should be remembered that the force dynamometer housing and the vibrator table are the parameters of a multi-degree-of-freedom system. The mass of the system has already been minimized and, if the stiffness of the linkages is high, then the resonant frequencies of the system will be well above the operating frequency range so that the motion of the dynamometer and vibrator table can be considered synonymous.

With all the above design criteria considered the design data works out as follows:

$$\begin{aligned}
 R_n &= 0.0095 \text{ m (3/8 in.)} & m_2 &= 0.29 \text{ kgm} \\
 \alpha &= 8 & m_1 &= 3.05 \text{ kgms} \\
 t_m &= 0.0016 \text{ m (1/16 in.)} & k_c &= 6.79 \times 10^8 \text{ N/m} \\
 T_s &= 0.0111 \text{ m (7/16 in.)} & k_t &= 9.2 \times 10^5 \text{ N/m} \\
 b &= 0.508 \text{ m (2.0 in.)} & \omega_t &= 83 \text{ Hz}
 \end{aligned}$$

Theory. The basic tool control system is represented in Figure 7. Let the power amplifier, electromagnetic vibrator and force dynamometer be represented by the following respective transfer functions:

$$\begin{aligned}
 T_1(s) &= \frac{v^i}{v} = G \\
 T_2(s) &= \frac{x}{v^i} = T \\
 T_3(s) &= \frac{v_o}{x} = \frac{1}{ms^2 + fs + k}
 \end{aligned} \tag{18}$$

where the dynamometer is considered as a single-degree-of-freedom system of mass (m), damping (f) and stiffness (k). The amplifier has a gain (G) and

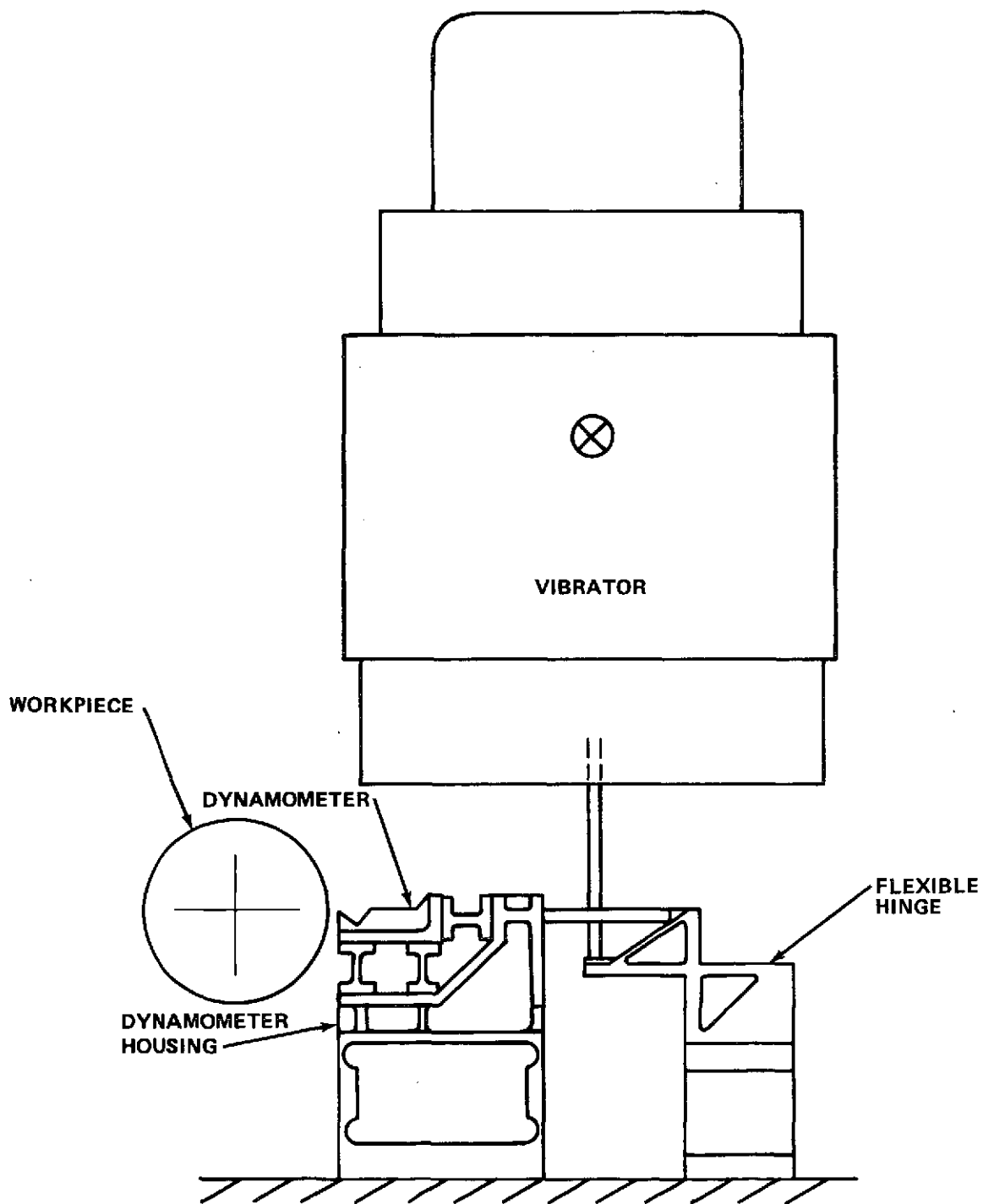


Figure 9. Schematic arrangement of the vibrator and flexible tooling.

the vibrator causes a displacement (Tv') for (v') volts input, s is a frequency operator, v a voltage and x a displacement.

The overall open loop response therefore becomes:

$$\frac{v_o}{v} = T_1(s) \cdot T_2(s) \cdot T_3(s) = \frac{TG}{ms^2 + fs + k} \quad (19)$$

For a linear system, if $v = e^{ist}$ and $v_o = Ae^{i(st+\phi)}$ in the steady state, then:

$$\frac{v_o}{v} = Ae^{i\phi} \quad (20)$$

where A and ϕ are both functions of frequency (s).

The stability of the system can now be examined by plotting the open loop amplitude (A)/phase (ϕ) response over the entire frequency range and examining its relationship with the Nyquist $(-1, 0)$ stability criterion; i.e., $A=1$, $\phi=-180^\circ$. It should be noted that equation (19) is an idealized solution depicting the major mode of vibration, but in the real case higher frequency modes may exist that could lead to instability.

Closing the loop with just a displacement feedback gives:

$$\frac{v_o}{v_i} = \frac{TG}{ms^2 + fs + (k + TG)} \quad (21)$$

whereas adding velocity feedback modifies equation (21) to:

$$\frac{v_o}{v_i} = \frac{TG}{ms^2 + (f + TG)s + (k + TG)} \quad (22)$$

Examining equations (21) and (22) shows that the addition of velocity feedback increases the system's damping and, hence, stability.

The closed-loop system can be described in a similar manner to the open-loop system of equation (20) by writing:

$$\frac{v_o}{v_i} = M e^{i\lambda} \quad (23)$$

where for a linear system $v_i = e^{ist}$ and $v_o = M e^{i(st + \lambda)}$ are in the steady state, and M and λ are both functions of frequency (s). The closed loop response can now be plotted in terms of frequency in a similar manner to the open loop, but more important is the ability to predict the closed loop response from the open loop response of equation (20). This is done realizing that the error signal (v) is the difference between the control signal (v_i) and the feedback signal (v_o). This gives:

$$\frac{v_o}{v_i} = \frac{v_o}{v} \left/ \left(1 + \frac{v_o}{v} \right) \right. \quad (24)$$

and combining equations (20), (23) and (24) the following relationship can be established:

$$\begin{aligned} M &= \frac{A}{\sqrt{A^2 + 2A \cos \phi + 1}} \\ \lambda &= \tan^{-1} \left(\frac{\sin \phi}{A + \cos \phi} \right) \end{aligned} \quad (25)$$

The system's open loop response will be examined next and the results used in conjunction with equation (25) to predict the closed loop response.

Open Loop Tests. The open loop response for the system shown schematically in Figure 7 is shown for displacement feedback only in Figure 10. The results are presented in the form of a Nyquist diagram described by

equation (20). It can be seen that the feedback/input ratio (v_o/v) is greater than unity over the frequency range 5 to 180 Hz and that there is a potential instability at 200 Hz that limits any further increase in gain. A further resonance at 670 Hz was attributed to a linkage resonance but being outside the required frequency range and in-phase it was of no consequence.

The open loop response for velocity feedback only is shown in Figure 11. The frequency range when v_o/v is greater than unity is seen to be 40 to 250 Hz. The main difference between this response and the one of Figure 10 is the poor low frequency response and the inclusion of some high frequency resonances at 1910 Hz, 2680 Hz and 2930 Hz attributed to be vibrator table and linkages resonances.

Combining the two types of feedback results in a good low frequency response and overcomes the potential 200 Hz instability of the displacement feedback system. This is shown to be the case in Figure 12, where v_o/v is greater than unity for the range 0 to 350 Hz and is limited only by the potential 4000 Hz instability.

The major high frequency modes can be substantially eliminated by modifying the velocity feedback function, first, by adding a high frequency filter with a cut off at about 1000 Hz; i.e., a first order filter, and second, by using a notch filter tuned to about 2800 Hz. It should be noted that filtering tends to introduce phase lag into the system and can cause instabilities at other frequencies. With the above modifications the system response is significantly improved as shown in Figure 13. The extent of control with a gain margin of 0.5 and phase margin of 30 deg is given in Table 1.

TABLE 1. FREQUENCY RANGE FOR WHICH THE OPEN LOOP RESPONSE EXCEEDS THE GIVEN VALUES OF

$$v_o/v$$

$\frac{v_o}{v}$	Frequency Range (Hz)	
	Low	High
10	50	140
5	0	200
2	0	350
1	0	500

The control, therefore, between 0 to 200 Hz is excellent while the remaining frequency range has a feedback/input ratio (v_o/v) of approximately two. This is a considerable improvement on the original unmodified system.

Closed Loop Tests. The open loop results of Figure 13 are used in conjunction with equation (25) to predict the closed loop response. This is done during the design stage to avoid unnecessary instabilities damaging the system when the loop is closed.

The measured results and those calculated from Figure 13 are compared in Figure 14 and show good correlation. It can be seen that the control signal amplitude and phase are held very well up to 200 Hz. The control above 200 Hz slowly reduces as the value of v_0/v , given in Table 1, drops with increased frequency.

CONCLUSIONS

A highly sensitive force dynamometer with temperature stability has been developed to measure machining forces in two mutually perpendicular directions with no cross sensitivity from one direction to the other.

The force dynamometer has been incorporated as the toolholder (Fig. 15) in a control system where the cutting tool oscillates in a controlled sinusoidal manner independently from the machining forces acting on the tool and unaffected by the response of the machine tool structure.

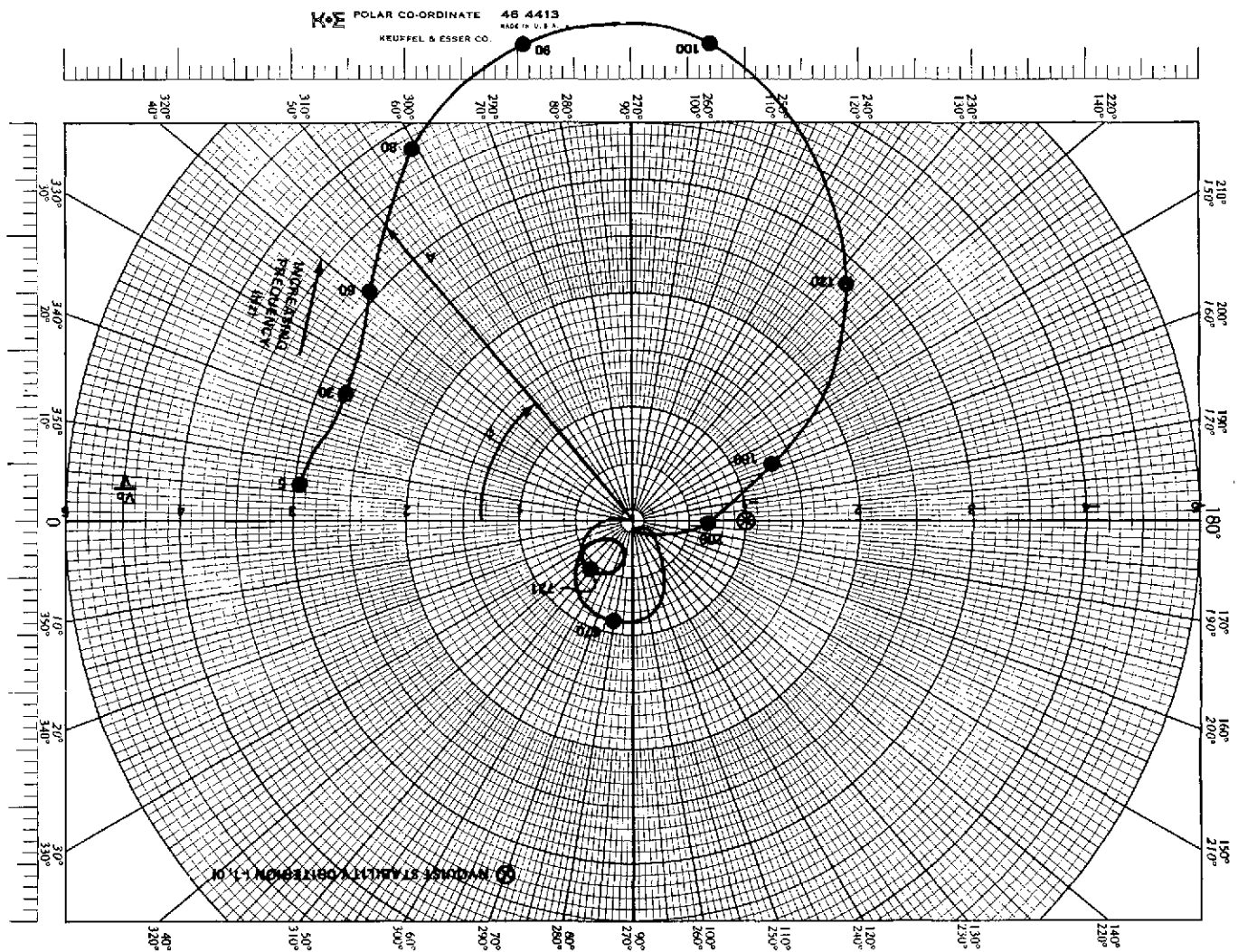


Figure 10. System response with displacement feedback only.

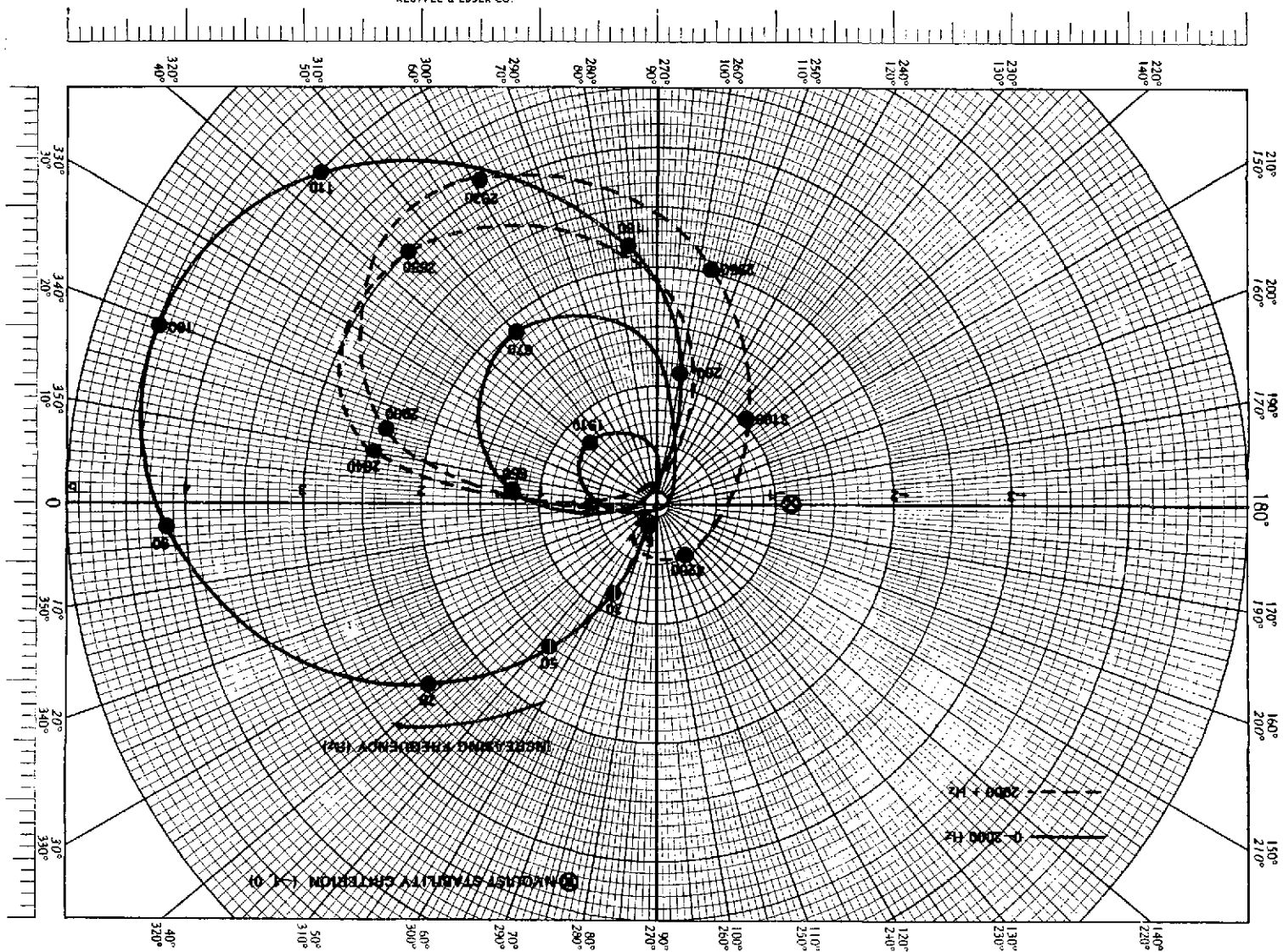


Figure 11. System response with velocity feedback only.

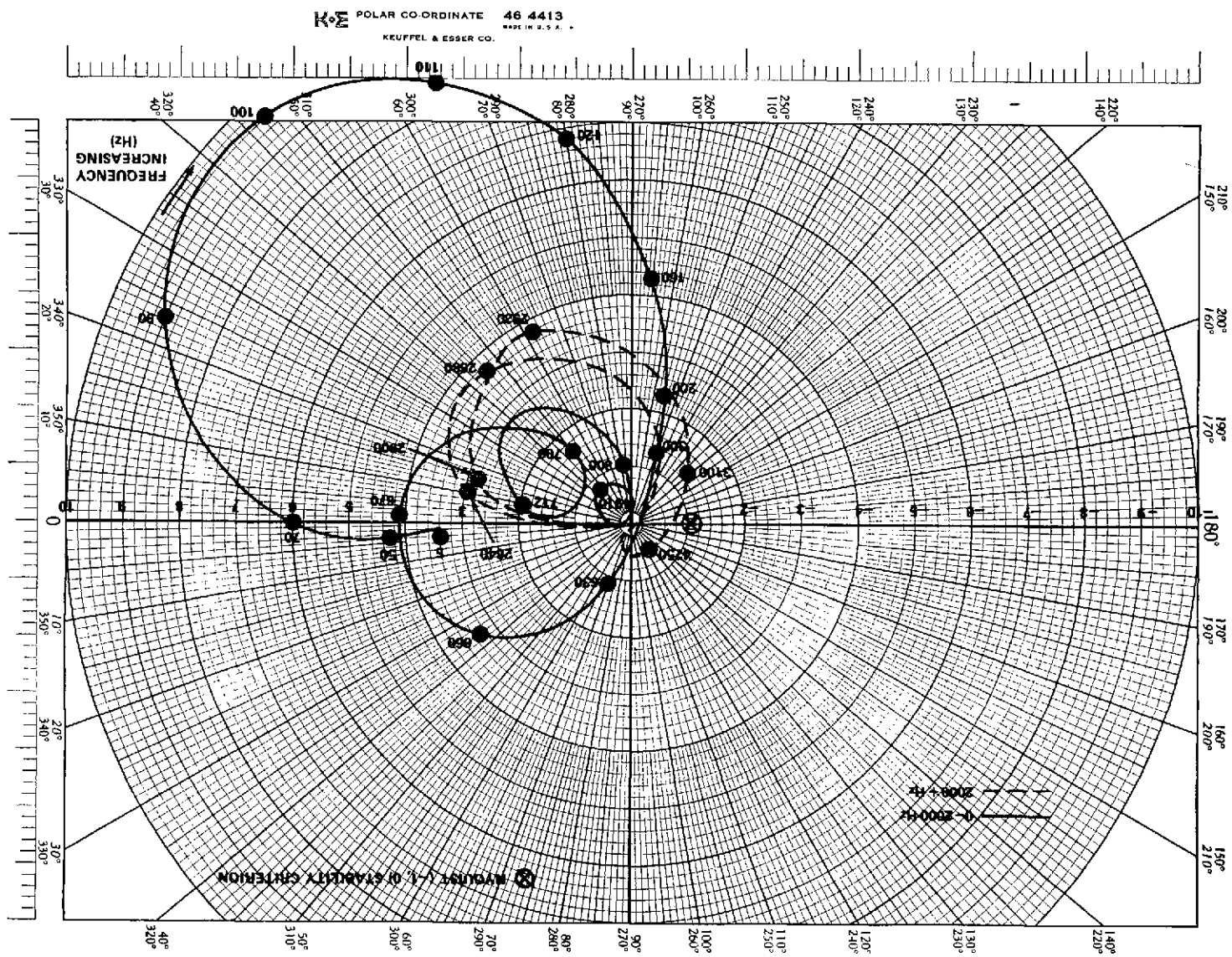


Figure 12. System response with displacement and velocity feedback.

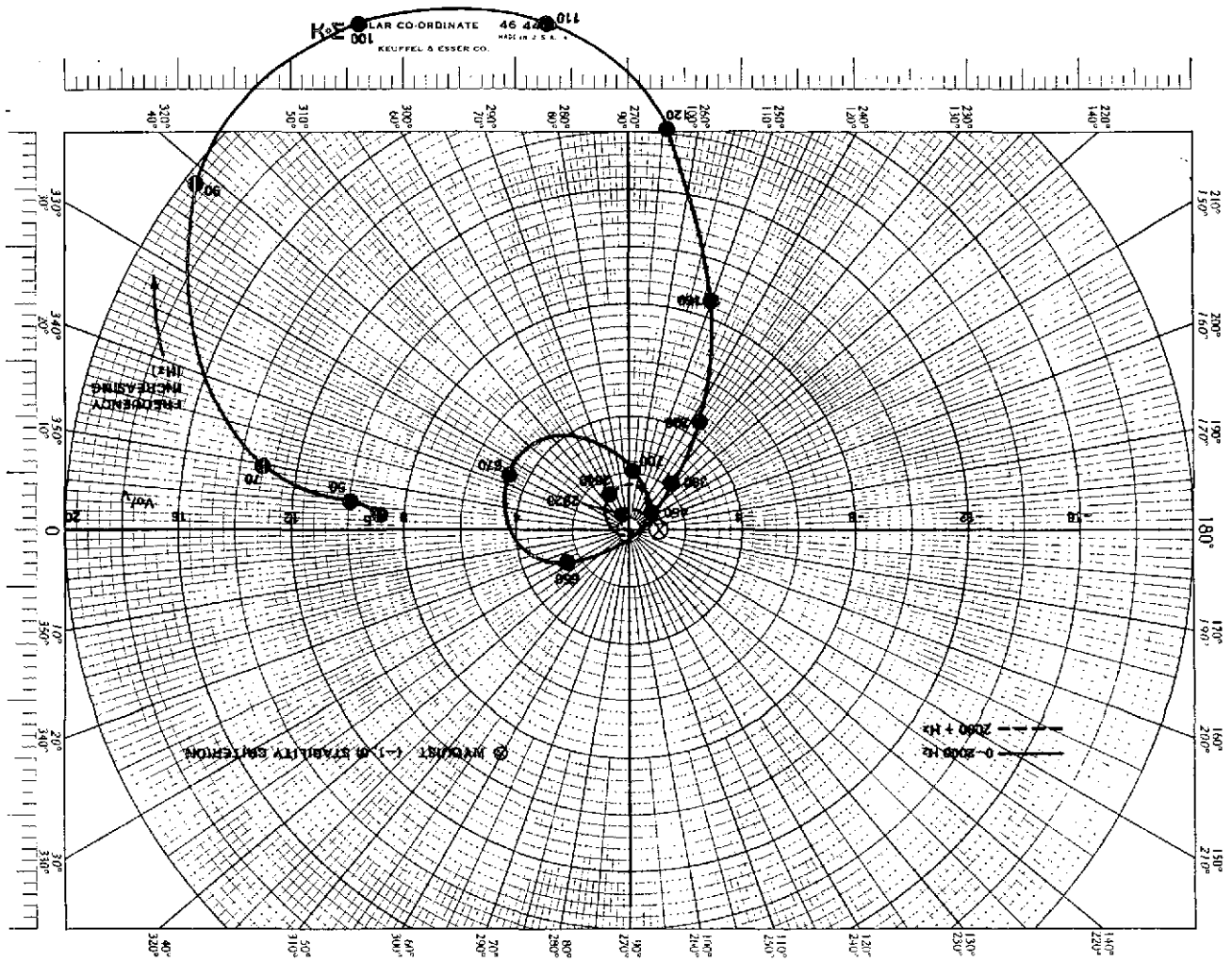


Figure 13. System response with displacement and velocity feedback — after modification.

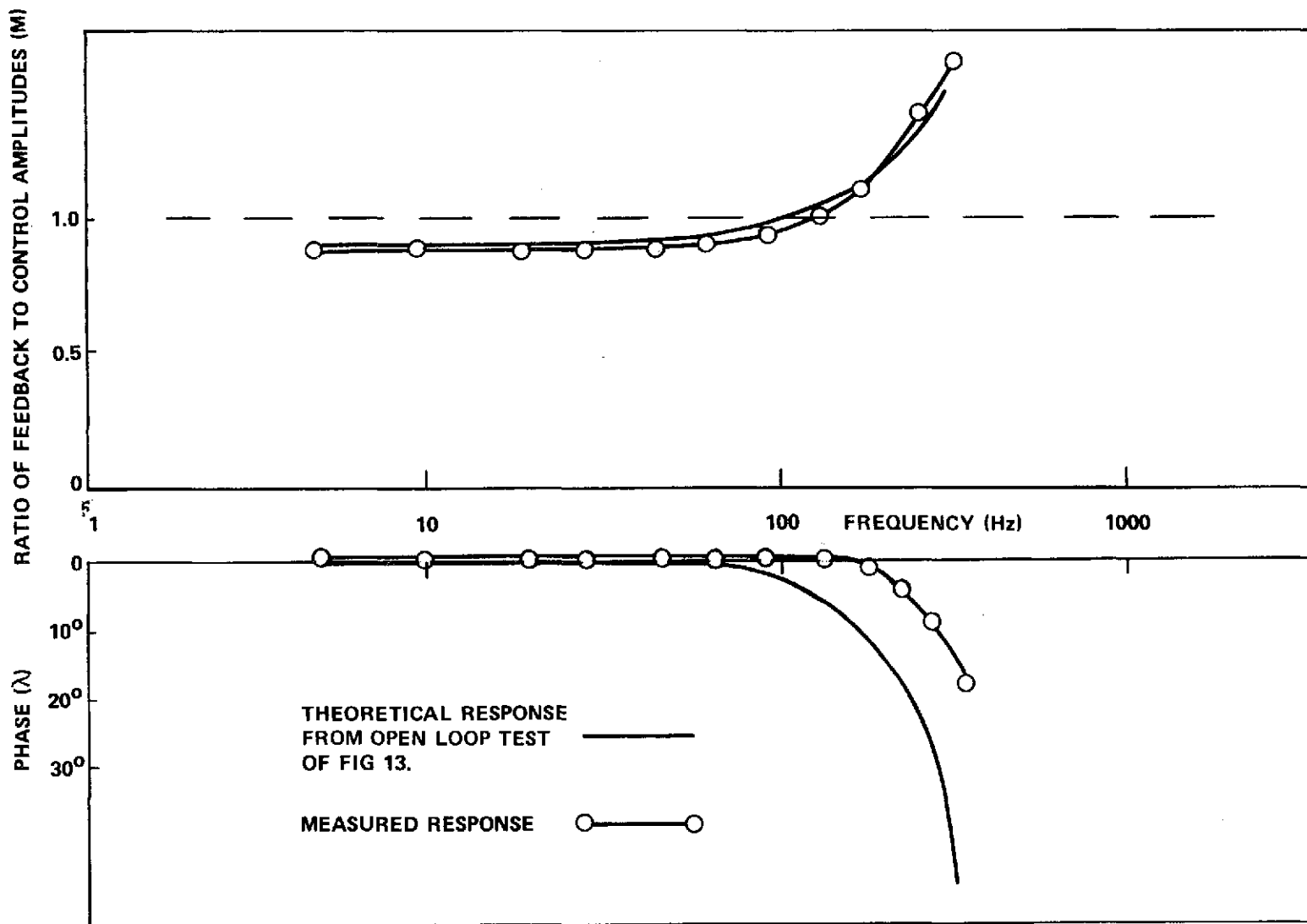


Figure 14. Closed loop response — comparing measured results with predicted.

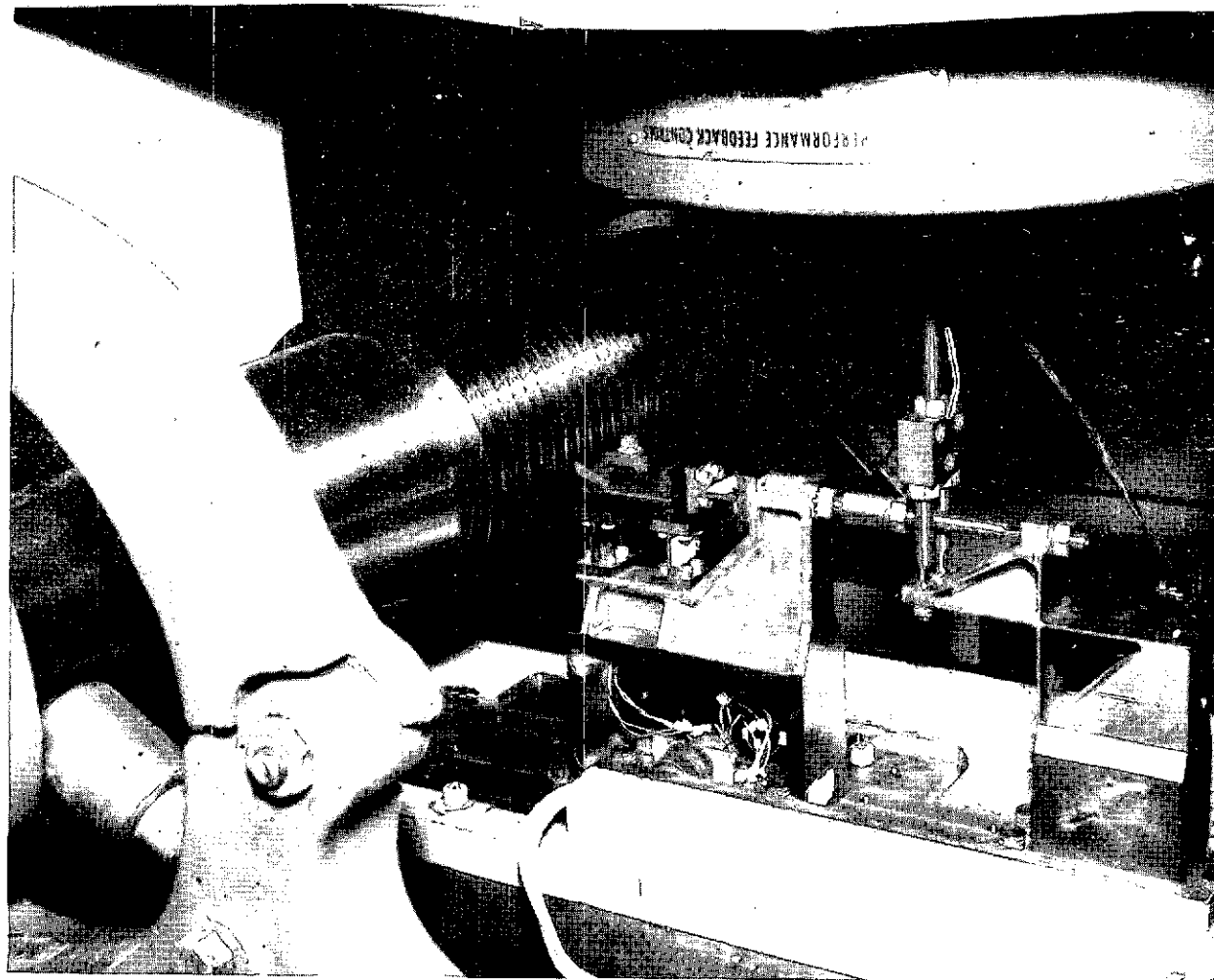


Figure 15. View of force dynamometer and flexible tooling showing completed assembly.

APPENDIX A

CALCULATION OF THE COMPRESSIVE AND BENDING STIFFNESSES OF THE FORCE DYNAMOMETER HOUSING

Compressive Stiffness (k_{cp})

The central compressive stiffness of the dynamometer housing illustrated in Figure 8 is given by:

$$k_{cp} = 2F/D \quad (A-1)$$

where F is the applied force and D is the total deflection of one strut. It should be noted that the compressive stiffness of the tool due to its overhang is approximately a factor 2.5 less than the above value.

The total strut deflection is given by:

$$D = 2d_n + d_s \quad (A-2)$$

where d_n is the deflection of a notch and d_s the deflection of the central portion of the strut shown in Figure 8. Let us consider first the deflection d_n of the notch.

The strain in an element of thickness (δy) in Figure A-1 is F/btE , where t is the thickness at a distance y from the end of the strut. To simplify the mathematics with little error a parabolic approximation is used for the notch form:

$$t = t_m + \frac{(y - R_n)^2}{R_n} \quad (A-3)$$

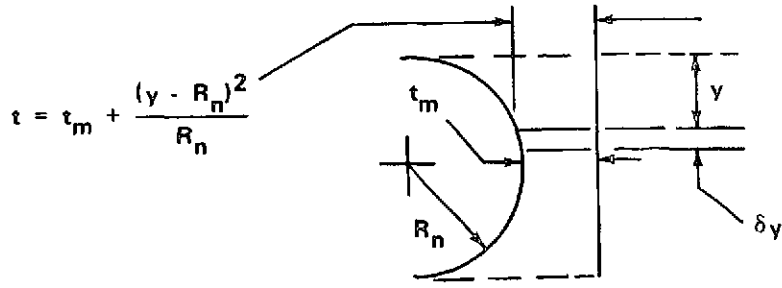


Figure A-1. Notch geometry.

The total deflection of the notch therefore is given by:

$$\begin{aligned}
 d_1 &= \frac{F}{bE} \int_0^{2R_n} \frac{R_n dy}{R_n t_m + (y - R_n)^2} \\
 &= \frac{2FR_n}{aEb} \tan^{-1} (R_n/a)
 \end{aligned} \tag{A-4}$$

where $a = \sqrt{R_n t_m}$.

The strain in the central portion is $F/bT_s E$ so that (d_s) is given by:

$$d_s = \frac{F\alpha R_n}{bT_s E} \tag{A-5}$$

Substitution in equations (A-1) and (A-2) gives:

$$k_{cp} = \frac{2bE}{R_n \left[(4/a) \tan^{-1}(R_n/a) + \alpha/T_s \right]} \tag{A-6}$$

Bending Stiffness (K_b)

The bending moment assuming that the strut is encastré at each end is given by:

$$M = F(L/2 - y) \quad (A-7)$$

The bending stiffness is calculated in a similar way to the compressive stiffness by considering each element separately. The mathematics, however, although not complicated, is tedious and will be omitted.

With reference to the notation of Figure 8, the bending stiffness of the strut is given by:

$$k_b = \frac{2}{\left[\frac{P}{(a^2 + R_n^2)^2} + \frac{Q}{(a^2 + R_n^2)} + S \tan^{-1}(R_n/a) + \frac{R_n^3 \alpha^3}{EbT_s^3} \right]} \quad (A-8)$$

where

$$P = \frac{12R_n^4}{Eb} \left[\frac{(L/2 - R_n)^2}{a^2} - 1 \right]$$

$$Q = \frac{6R_n^3}{Ebt_m} \left[\frac{3(L/2 - R_n)^2}{a^2} + 1 \right]$$

$$S = Q/aR_n \quad ; \quad a = \sqrt{R_n t_m}$$

APPENDIX B

DESIGN OF FLEXIBLE HINGE

The hinge is designed purely to transfer motion from one axis to another with no mechanical backlash that could lead to instabilities in a servo control loop. Motion is transferred from the vibrator axis to the tool axis as shown in Figure B-1 by means of a pair of mutually perpendicular struts. The combined torsional stiffness (k_{tr}) of the strut combination is given by:

$$k_{tr} = \frac{Ebd^3}{6l} \quad (B-1)$$

and the compressive stiffness (k_{cp}) by:

$$k_{cp} = \frac{Ebd}{l} \quad (B-2)$$

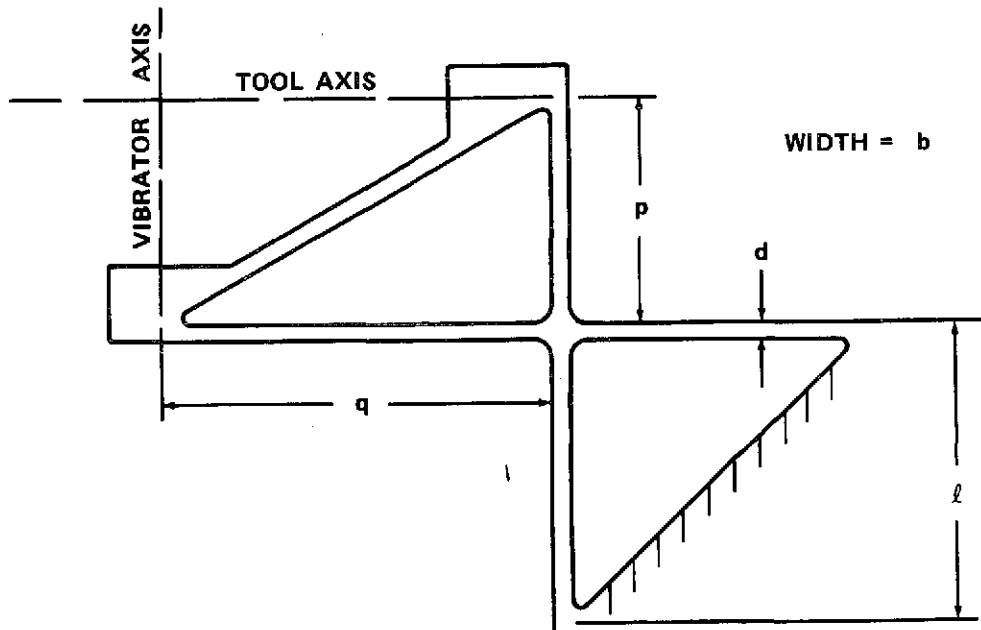


Figure B-1. Flexible hinge geometry and notation.

The effective stiffness of the hinge along the tool axis should be at least a factor ten below the bending stiffness of the force dynamometer housing so that the natural frequency of the system that has already been established is not significantly modified, so that $k_{tr} = k_b p^2/10$. The compressive stiffness should be at least 2.5×10^8 N/m to ensure only torsional movement of the hinge. Combining equations (B-1) and (B-2):

$$\frac{\text{Torsional Stiffness } (k_{tr})}{\text{Compressive Stiffness } (k_{cp})} = \frac{d^2}{6} = \frac{p^2 k_b}{10 k_{cp}} = \frac{9 \times 10^5 \cdot p^2}{10 \times 2.5 \times 10^8}$$

so that

$$p = 21.5d \quad (B-3)$$

Substituting values for E and k_{cp} in equation (B-2) gives a relationship between b, l and d:

$$l = 800db \quad (B-4)$$

There are a number of solutions possible from equations (B-3) and (B-4) but the most convenient for the present configuration gives the following geometry:

$$p = 0.0375m \quad (1.5 \text{ in.})$$

$$b = 0.0375m \quad (1.5 \text{ in.})$$

$$d = 0.0016m \quad (1/16 \text{ in.})$$

$$l = 0.050m \quad (2.0 \text{ in.})$$

The remaining dimension to establish is the moment arm (q) of the vibrator axis about "O" in Figure B-2. This is optimized by considering the total inertia of the vibrating system.

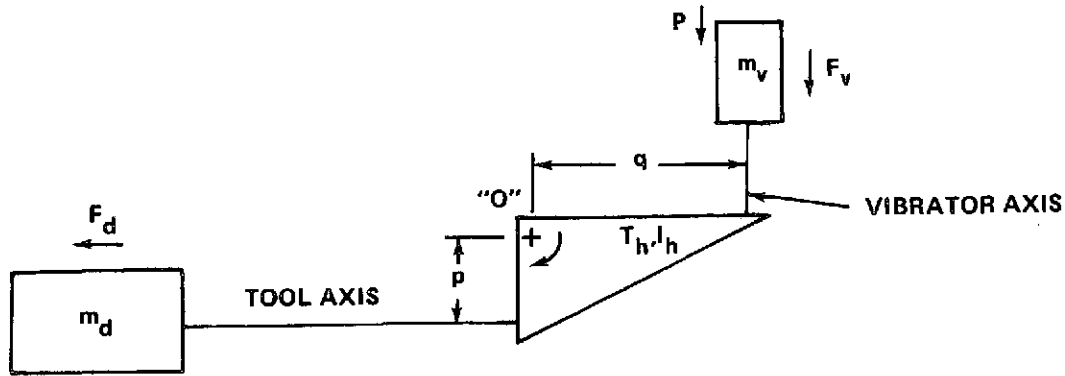


Figure B-2. Notation of vibrating system.

Taking moments about "O":

$$qP = pF_d + T_h + qF_v \quad (B-5)$$

where

$$F_d = X_d m_d \omega^2$$

$$T_h = I_h \Theta_h \omega^2$$

$$F_v = X_v m_v \omega^2$$

and m is mass, X is displacement, ω angular frequency and P the vibrator output force.

Considering the hinge angular rotation (Θ_h) in relation to the displacements X_d and X_v of the dynamometer and vibrator table respectively:

$$\Theta_h = \frac{X_v}{q} = \frac{X_d}{p}$$

so that:

$$X_v = \frac{qX_d}{p} \quad (B-6)$$

Substitution in equation (B-5) gives:

$$p = X_d M^* \omega^2 \quad (B-7)$$

where M^* is the equivalent mass of the system as seen by the vibrator and is given by:

$$M^* = \left[\frac{pm_d}{q} + \frac{I_h}{pq} + \frac{qm_v}{p} \right] \quad (B-8)$$

This mass is a minimum when:

$$q = \sqrt{\frac{m_d}{m_v}} \cdot p \quad (B-9)$$

If $p = 0.0375m$ (1.5 in.), $m_d = 3$ kgm and $m_v = 1$ kgm, then q becomes approximately $0.0625m$ (2.5 in.).

The inertia of the hinge is minimized by machining away redundant material to reduce the second moment of area term (I_h) in equation (B-8).

If the force requirements of the vibrator need to be calculated, then equation (B-7) can be used to represent the system inertia.

REFERENCES

1. Kegg, R. L.: Cutting Dynamics in Machine Tool Chatter — Contribution to Machine Tool Chatter Research. *Journal of Engineering for Industry*, 87B, 464, 1965.
2. Komanduri, R.; Stewart, V. A.; and Brown, R. H.: Dynamic Calibration of Dynamometers. *Annals of the C. I. R. P.*, vol. XIV, pp. 231 through 236, 1971.
3. Sutherland, I. A.: Forced Vibration, Chatter and Surface Finish in Horizontal Milling. PhD thesis, Bristol University, England. pp. 27 through 32, 1971.
4. Wallace, P. W.; and Andrew, C.: Machining Forces — Some Effects of Tool Vibration. *Journal of Mechanical Engineering Science*, vol. 7, No. 2, p. 152, 1965.
5. Smith, J. D.; and Tobias, S. A.: The Dynamic Cutting of Metals. *International Journal of Machine Tool Design and Research*, vol. 1, pp. 283 through 292, 1961.


APPROVAL

THE DEVELOPMENT OF A TWO-COMPONENT FORCE DYNAMOMETER AND TOOL CONTROL SYSTEM FOR DYNAMIC MACHINE TOOL RESEARCH

By Ian Alexander Sutherland

The information in this report has been reviewed for security classification. Review of any information concerning Department of Defense or Atomic Energy Commission programs has been made by the MSFC Security Classification Officer. This report, in its entirety, has been determined to be unclassified.

This document has also been reviewed and approved for technical accuracy.


DR. M. P. L. ~~SIEBEL~~

8/1/73
Director, Process Engineering Laboratory

*U. S. Government Printing Office:-1973-748-291/80

Do not Reproduce

DISTRIBUTION

INTERNAL

DIR

DEP-T

A&PS-PAT

Mr. L. D. Wofford, Jr.

A&PS-MS-H

Mr. D. S. Akens

A&PS-MS-IP (2)

Mr. J. D. Ledbetter

A&PS-MS-IL (8)

Miss L. M. Robertson

A&PS-TU (6)

Mr. J. W. Wiggins

A&PS-MS-I

Mr. W. J. Ziak

AD-S

Dr. E. S. Stulinger

Dr. G. C. Bucher

PD-DIR

Mr. J. T. Murphy

PD-DO-DIR

Mr. E. Goerner

S&E-ASTR-G

Dr. F. S. Wojtalik

S&E-ASTR-M

Mr. J. Boehm

S&E-ASTR-IMP

Mr. H. S. Harman

S&E-ASTR-GD

Mr. C. S. Jones

S&E-ASTR-GDS

Mr. F. J. Nola

S&E-ASTN-E

Mr. G. Kroll

S&E-ASTN-M

Mr. R. Schwinghamer

S&E-QUAL-DIR

Dr. D. Grau

S&E-R-DIR

Dr. W. G. Johnson

S&E-PE-DIR

Dr. M. P. L. Siebel

Mr. H. F. Wuenscher

S&E-PE-D

Mr. F. Weckworth (2)

S&E-PE-T

Mr. W. G. Crompton

S&E-PE-P

Mr. W. S. Franklin

S&E-PE-M

Mr. W. Angele

S&E-PE-MX

Mr. P. M. Schuerer

S&E-PE-MW

Mr. P. G. Parks

S&E-PE-ME

Mr. J. D. Bennight

Mr. J. R. Rasquin

Mr. J. D. Hankins

S&E-PE-MEE

Mr. R. M. Avery

Mr. H. E. Smith

S&E-PE-MEP

Mr. L. C. Jackson

S&E-PE-MES

Mr. R. M. Herndon

Mr. C. Stocks

S&E-PE-MEI

Mr. W. A. Wall

Mr. R. Taylor

S&E-PE-PME

Mr. T. N. Vann

EXTERNAL

Associateship Office

Office of Scientific Personnel

National Research Council

2101 Constitution Avenue, N. W.

Washington, D. C. 20418

Attn: Dr. R. W. Kinney

Dr. T. H. Curry

Scientific & Technical Information

Facility (25)

P. O. Box 33

College Park, Md. 20740

Attn: NASA Representative (S-AK/RKT)

Hayes International Corporation

P. O. Box 1568

Huntsville, Alabama 35807

Attn: William T. Weissinger